J. Plasma Phys. (2023), *vol*. 89, 915890501
Published by Cambridge University Press

doi:10.1017/S0022377823000892

Numerical simulations of relativistic jets

Manel Perucho [1,2,†] **and J. López-Miralles** [1,3]

[1]Departament d'Astronomia i Astrofísica, Universitat de València, C/ Dr. Moliner, 50, 46100 Burjassot, Valencian Country, Spain

[2]Observatori Astronòmic, Universitat de València, C/ Catedràtic José Beltrán 2, 46980 Paterna, Valencian Country, Spain

[3]Aurora Technology for the European Space Agency, XMM-Newton Science Operations Center, ESAC/ESA, Camino Bajo del Castillo s/n, Urb. Villafranca del Castillo, 28691 Villanueva de la Cañada, Madrid, Spain

(Received 8 March 2023; revised 1 August 2023; accepted 8 August 2023)

In this paper, we review recent and ongoing work by our group on numerical simulations of relativistic jets. Relativistic outflows in astrophysics are related to dilute, high energy plasmas, with physical conditions out of the reach of current laboratory capabilities. Simulations are thus imperative for the study of these objects. We present a number of such scenarios that have been studied by our group at the Universitat de València. In particular, we have focused on the evolution of extragalactic outflows through galactic and intergalactic environments, deceleration by interaction with stars or clouds or the propagation of jets in X-ray binaries and interaction with stellar winds from massive companions. All also share their role as particle acceleration sites and production of non-thermal radiation throughout the electromagnetic spectrum. Therefore, our work is not only aimed at understanding the impact of outflows on their environments and thus their role in galaxy and cluster evolution, but also the nature and capabilities of these sites as generators of high- and very-high-energy radiation and cosmic rays.

Key words: astrophysical plasmas, plasma simulation

1. Introduction

Jets and outflows represent a common and crucial process in astrophysical systems; from forming stars (Herbig-Haro objects) to supermassive black holes in active galactic nuclei (AGN). In each of these systems, the properties of the jets (velocities, densities, composition…) are different, but they share a common association with accretion and magnetohydrodynamical processes that explain their formation, collimation and acceleration (see, e.g. Komissarov 2012).

We know that extragalactic, AGN jets, can be modelled as fluids or plasmas because the typical Larmor radius of the jet particles is orders of magnitude smaller than the spatial scales of the system (Blandford & Rees 1974). The same is true for the case of

† Email address for correspondence: manel.perucho@valencia.edu

jets generated in collapsars and X-ray binary stars. Despite technical advances, it is still impossible to reproduce the most extreme of these systems, i.e. to accelerate plasmas to relativistic velocities, in laboratories to study their properties (e.g. Bellan 2018).[1] This leaves numerical simulations as the only option to approach the nature of these systems, which can be central in the evolution of the interstellar medium in host galaxies and clusters (e.g. McNamara & Nulsen 2007; Fabian 2012), or in the generation of high and very high energy radiation in the Universe (e.g. Rieger & Levinson 2018).

Relativistic jets are formed in the environment of compact objects by the extraction of rotational energy from the accreting body and/or the accretion disk (Blandford & Znajek 1977; Blandford & Payne 1982). The idea is, in both cases, related to the twisting of magnetic field lines, which, by resisting this deformation, are able to extract rotational energy from the system. The magnetic field is supposed to be dragged onto the central object by the accreting gas itself. In the case of Kerr black holes, it anchors to the hole's ergosphere and is thus forced to rotate faster inside than outside of this region, which creates the aforementioned twisting (Blandford & Znajek 1977; Komissarov 2012).

In all cases, jet evolution involves many orders of magnitude in distance. In the case of AGN jets, jet formation takes place at spatial scales of the order of the gravitational radius of the central supermassive black hole, i.e. $\sim 10^{10}$ m, or, if the inner regions of the accretion disk are involved, it may extend to a factor 10–100 larger. They reach, in contrast, distances up to ~ 1 Mpc, i.e. $\sim 10^{22}$ m, as revealed by low frequency surveys (see, e.g. Icke 1991; Molina *et al.* 2014; Oei *et al.* 2022; Simonte *et al.* 2023). As a consequence, the computational resources required to study the whole evolution are prohibitive, even for modern architectures, and studies focus on different regions. Depending on this, the properties of the jets vary and the numerical codes have to be adapted to them.

When ejected, jets consist mainly of a Poynting flux, which may be loaded by a dilute, hot gas with an electron–positron pair composition the pairs would be generated by photon–photon collisions at the black hole corona and/or an electron–proton gas if loaded from the accretion disk. These jets are launched with a relatively small radial velocity. Taking into account the large values achieved by magnetic fields in these regions, their velocities must initially be sub-Alfvènic. Nevertheless, relativistic speeds are reported at sub-parsec to parsec scales, which means that jets need to be accelerated to super-Alfvènic (super-fast-magnetosonic) speeds. The mechanisms that are typically invoked to explain this acceleration are both related to jet expansion with magnetic and internal energy contributions (e.g. Vlahakis & Königl (2004), Komissarov *et al.* (2007) and Ricci *et al.*, in preparation).

At kiloparsec scales, jets show different morphologies and clear signs of interaction with the warm–hot intergalactic medium (WHIM, e.g. Croston *et al.* 2019). A coarse, initial dichotomy was established by Fanaroff & Riley (1974) between Fanaroff–Riley type I (FRI) sources and Fanaroff–Riley type II (FRII) sources. The former are brighter within their host galaxies, jets become dimmer with distance and show brightness symmetry at large distances (e.g. Laing & Bridle 2014). The FRIIs are brighter at the impact sites with the WHIM, the so-called hotspots, and show brightness asymmetry along their length between the jets and their counter-jets. The common interpretation is related to jet velocity: on the one hand, FRII jets seem to keep their collimation and mildly relativistic velocities up to the interaction site with the WHIM, which means that the flow is supersonic at impact, triggering strong shocks that show up as hotspots, where Doppler boosting explains the brightness asymmetry; on the other hand, in the case of FRI jets, the loss

[1] This would imply including enough particles to provide the system with fluid/plasma properties.

https://doi.org/10.1017/S0022377823000892 Published online by Cambridge University Press

of collimation and brightness symmetry at large scales point towards deceleration and weakening of the Doppler asymmetry (Bridle 1984; Bridle & Perley 1984).

In the case of microquasars, although jets evolve on time scales much shorter than AGN jets (see, e.g. Mirabel (2010) and Fender (2006), for a review), a large number of unknowns remain about fundamental aspects such as their composition (Migliari, Fender & Méndez 2002), internal dynamics and its relation to the formation mechanism and changes in the accretion flow (Fender, Belloni & Gallo 2004), or the mechanisms that generate the production of high- to very-high-energy radiative output within the binary scales (see, e.g. Perucho & Bosch-Ramon 2008; Bosch-Ramon & Khangulyan 2009*a*; Perucho, Bosch-Ramon & Khangulyan 2010*a*; Bosch-Ramon *et al.* 2012*a*; Perucho & Bosch-Ramon 2012; Bosch-Ramon, Barkov & Perucho 2015; Paredes-Fortuny *et al.* 2015; de la Cita *et al.* 2017; López-Miralles *et al.* 2022), even far from the sub-milliarscsecond resolution achieved by very large baseline interferometry at cm–mm wavelengths in the radio band. Furthermore, the transition of the jet from these compact regions ($\sim 10^{10}$ m) to parsec scales ($\sim 10^{16}$ m) has been barely studied by numerical simulations, and only few works have been devoted to microquasar jet evolution at the largest scales (e.g. Bordas *et al.* 2009; Monceau-Baroux *et al.* 2015; Charlet *et al.* 2022).

In all scenarios in which relativistic outflows are involved, and once accelerated, the jets are subject to dissipative processes such as shocks or mass entrainment via interaction with stars and the development of instabilities (Perucho 2019). The remarkable stability of jets on the different scales through which many of them are observed to propagate has been a matter of study during the last decades. The mechanisms by which extragalactic FRI jets are decelerated have also been deeply investigated (e.g. Perucho *et al.* 2014; Massaglia *et al.* 2016, 2019, 2022; Gourgouliatos & Komissarov 2018; Perucho 2020; Anglés-Castillo *et al.* 2021). Attention has been paid to the scenarios of generation of high-energy particles (e.g. neutrinos, see Murase & Stecker 2022; Buson *et al.* 2023) and cosmic rays in these systems, both in galactic and extragalactic sources (e.g. Rieger & Levinson 2018; Matthews, Bell & Blundell 2020; Seo, Ryu & Kang 2022 and references therein). The particles could be accelerated via shock or shear acceleration, or also magnetic reconnection processes, i.e. as a byproduct of jet development. Recent works based on particle-in-cell simulations suggest a relation between synchrotron light polarization and jet composition (e.g. Meli & Nishikawa 2021). It is relevant to stress that a baryonic component is necessary to explain the generation of neutrinos, for instance. This component could be either provided by a disk-generated wind surrounding the inner leptonic jet spine, or by entrainment. Finally, the role of jets in heating galactic environments, avoiding the fast cooling and collapse of the WHIM onto the jet's host galaxy, also known as a feedback process, could be very relevant in galaxy evolution and is not only part of research on jet physics, but also on cosmological simulations (e.g. Tremmel *et al.* 2017; Weinberger *et al.* 2017; Vazza *et al.* 2023).

In this paper, we summarize our recent work on jet physics, which is mainly focused on jet propagation, stability and interaction with the ambient medium at different scales in both extragalactic sources and X-ray binaries, via numerical simulations, and also present new results either based on revisiting published work or on new simulations. In § 2, we present the basic equations that need to be solved to simulate the evolution and physics of these systems, and the numerical techniques that we use to solve them. Section 3 is devoted to the different applications that we have performed in the last years, both in the case of relativistic hydrodynamics (RHD) and magnetohydrodynamics (RMHD), and the main results that we have obtained. Among these, we include new results such as the pseudo-synchrotron images derived from AGN jet simulations (figures 1 and 2 in § 3.1.1), and the new simulations on jet–interstellar medium (ISM) interactions (§ 3.1.3) as well as

https://doi.org/10.1017/S0022377823000892 Published online by Cambridge University Press

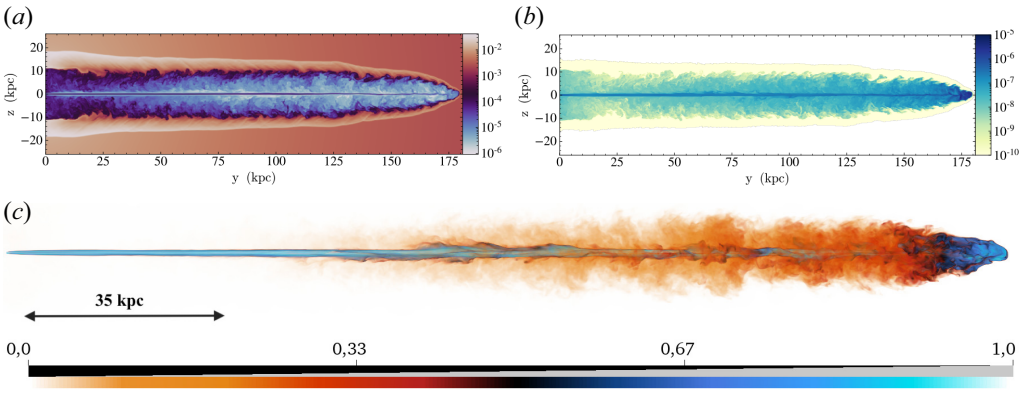

FIGURE 1. (*a*) Rest-mass density (units: $\rho_a = 1.7 \times 10^{-22}\,\mathrm{kg\,m^{-3}}$) cut. (*b*) Pressure weighted by tracer (units: $\rho_a c^2 = 1.6 \times 10^{-5}\,\mathrm{Pa}$). (*c*) Tracer rendering (jet mass fraction, ranging between 0 for the ambient gas and 1 for the jet gas).

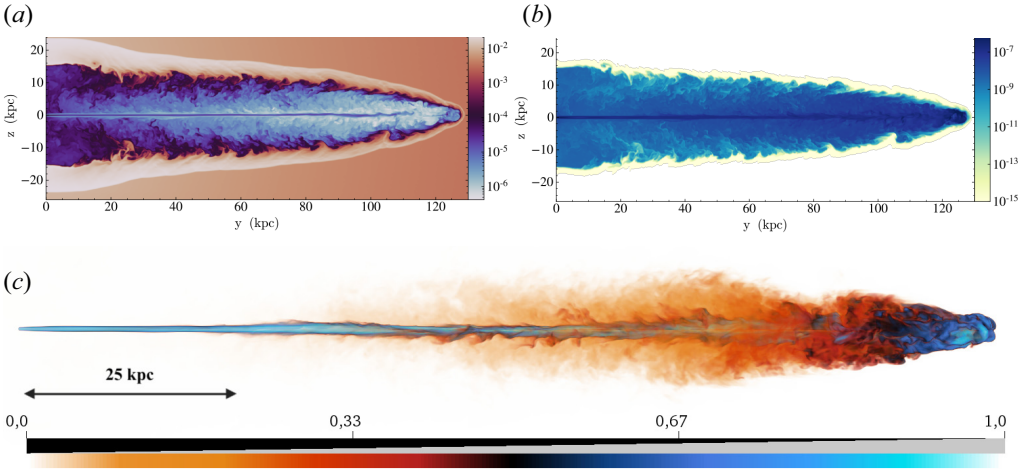

FIGURE 2. (*a*) Rest-mass density (units: $\rho_a = 6.8 \times 10^{-22}\,\mathrm{kg\,m^{-3}}$) cut. (*b*) Pressure weighted by tracer (units: $\rho_a c^2 = 6.4 \times 10^{-5}\,\mathrm{Pa}$). (*c*) Tracer rendering (jet mass fraction, ranging between 0 for the ambient gas and 1 for the jet gas). This figure shows the result from a simulation with the same jet properties as those of the jet shown figure 1, but with a factor 4 denser ambient medium.

a new analysis of recent RMHD simulations (§ 3.2). Finally, our conclusions are given in § 4.

2. Numerical codes and methods

2.1. *The RMHD equations*

The stress–energy tensor for an ideal plasma is $T^{\mu\nu} = T^{\mu\nu}_G + T^{\mu\nu}_{EM}$. On the one hand, the gas contribution is given by

$$T^{\mu\nu}_G = \rho h u^\mu u^\nu + p g^{\mu\nu}, \tag{2.1}$$

where the Greek letters take values $\mu,\ \nu = 0, 1, 2, 3$ and stand for the dimensions of the Minkowski space–time, ρ is the flow rest-mass density, h the gas specific enthalpy, u is the

https://doi.org/10.1017/S0022377823000892 Published online by Cambridge University Press

four-velocity, p is the gas pressure and g the Minkowski metric, and we have used $c = 1$. On the other hand, the field contribution is given by

$$T^{\mu\nu}_{EM} = F^{\mu}_{\beta} F^{\nu\beta} - \tfrac{1}{4} g^{\mu\nu} F_{\alpha\beta} F^{\alpha\beta}, \tag{2.2}$$

where $F^{\alpha\beta} = \epsilon^{\alpha\beta\mu\nu} b_{\mu} u_{\nu}$ are the elements of the electromagnetic field tensor satisfying the Maxwell equations

$$\partial_{\alpha} F_{\mu\nu} = 0, \quad \nabla_{\mu} F^{\mu\nu} = -J^{\nu}. \tag{2.3a,b}$$

In this expression $\epsilon^{\alpha\beta\mu\nu}$ is the Levi-Civita tensor, b_{μ} are the components of the magnetic field in the fluid rest frame and J^{ν} is the charge four-current. Collecting the expressions above, we obtain the stress–energy tensor of a magnetized, perfect fluid

$$T^{\mu\nu} = \rho h^{*} u^{\mu} u^{\nu} + p^{*} g^{\mu\nu} - b^{\mu} b^{\nu}, \tag{2.4}$$

where $h^{*} = h + |b|^2/\rho$ is the total enthalpy, p^{*} the total (gas plus magnetic) pressure ($p^{*} = p_{\rm gas} + |b|^2/2$), b^{μ} is the relativistic magnetic field four-vector, with $b^0 = \gamma(\boldsymbol{v} \cdot \boldsymbol{B})$, and $b^i = B^i/W + v^i b^0$, so $|b|^2 = b_{\alpha} b^{\alpha} = B^2/\gamma^2 + (\boldsymbol{v} \cdot \boldsymbol{B})^2$, with $\boldsymbol{B}$, $\boldsymbol{v}$ the magnetic field and velocity vectors in the laboratory frame, and γ is the corresponding Lorentz factor. We note that a $\sqrt{4\pi}$ factor is included in the definition of the magnetic fields.

The conservation laws that govern the dynamics of the plasma are

$$\nabla_{\mu} T^{\mu\nu} = 0, \quad \nabla_{\mu} (\rho u^{\mu}) = 0. \tag{2.5a,b}$$

These equations can be written in matrix form as

$$\partial_t \boldsymbol{U} + \partial_i \boldsymbol{F}^i = 0, \tag{2.6}$$

where $\boldsymbol{U} = \{D, S^j, \tau_e, B^j\}$ is a vector of conserved variables, D is the relativistic rest-mass density, S^j is the momentum density of the magnetized fluid, τ_e is the energy density and $\boldsymbol{F}^i$ are the fluxes in each spatial direction. The relation of those conserved quantities and fluxes to their primitive physical variables is given by

$$\boldsymbol{U} = \begin{pmatrix} D \\ S^j \\ \tau_e \\ B^j \end{pmatrix} = \begin{pmatrix} \rho\gamma \\ \rho h^{*} \gamma^2 v^j - b^0 b^j \\ \rho h^{*} \gamma^2 - p^{*} - b^0 b^0 - \rho\gamma \\ B^j \end{pmatrix}, \tag{2.7}$$

$$\boldsymbol{F}^i = \begin{pmatrix} \rho\gamma v^i \\ \rho h^{*} \gamma^2 v^i v^j + p^{*} \delta^{ij} - b^i b^j \\ \rho h^{*} \gamma^2 v^i - b^0 b^i - \rho\gamma v^i \\ v^i B^j - B^i v^j \end{pmatrix}. \tag{2.8}$$

Finally, from (2.3*a*,*b*), we obtain the divergence-free condition for the magnetic field, $\nabla \cdot \boldsymbol{B} = 0$.

This system of equations needs to be closed by means of an equation of state. It is common to use the ideal gas equation of state for this purpose. However, in the case of relativistic outflows propagating through their host galaxies, the different compositions of the jet flow (electron/positron pairs and/or electron/proton) and the ambient medium (ionized hydrogen in the intergalactic medium, but also atomic hydrogen in two phase media such as the ISM) recommend the use of the relativistic gas equation of state (Synge 1957).

https://doi.org/10.1017/S0022377823000892 Published online by Cambridge University Press

Source terms can be added to the equations, depending on the problems to be solved. Typical source terms used are gravity (or pseudo-gravity to keep a density/pressure profile in equilibrium, e.g. Perucho & Martí 2007; Perucho, Martí & Quilis 2019), thermal cooling terms (e.g. Perucho, Bosch-Ramon & Barkov 2017*a*), hydrogen ionization and recombination effects (e.g. Vaidya *et al.* (2015), Perucho *et al.* (2021), Perucho *et al.*, in preparation) or radiation feedback (López-Miralles, Martí & Perucho 2023).

It is worth noting that, on the one hand, relativistic effects arise when $v \to c$ and/or when $\varepsilon \to c^2$, and, on the other hand, magnetic fields can be dynamically relevant for even small values of the magnetic parameter $\sigma = |b^2|/(\rho h)$, which gives the ratio of magnetic to gas kinetic energy.

2.2. *The numerical codes*

Numerical codes are aimed at solving the RMHD equations (see Martí & Müller (2015) and Martí (2019) for reviews). In our case, we use multi-dimensional high resolution shock-capturing methods, with a finite volume scheme. Time advance of the equations is done via dimensional splitting to compute the numerical fluxes across cell boundaries, using the integral form of the conservation equations (see e.g. Komissarov 1999) and Runge–Kutta methods (Shu & Osher 1989).

In the case of RHD simulations, we use our code RATPENAT, a hybrid parallel code – MPI + OpenMP – (see Perucho *et al.* (2010*b*) and references therein) in which: (i) primitive variables within numerical cells are reconstructed using piecewise-parabloic method (PPM) routines, (ii) numerical fluxes across cell interfaces are computed with the Marquina flux formula, (iii) advance in time is performed with third-order total variation diminishing (TVD)-preserving Runge–Kutta methods.

The RMHD simulations are run with the code LÓSTREGO (López-Miralles *et al.* 2022), which uses the same basic strategy, although with different schemes: (i) primitive variables are reconstructed using piecewise linear methods: MinMod (Roe 1986), monotonized central (MC) (van Leer 1977) or VanLeer (van Leer 1974), with slope limiters that preserve monotonicity (Suresh & Huynh 1997), (ii) the approximate solvers used to compute the fluxes are Harten-Lax-Van Leer (HLL) (Harten, Lax & van Leer 1983), HLLC (Mignone & Bodo 2006) and HLLD (Mignone, Ugliano & Bodo 2009). In this case, the divergence-free condition of the field is maintained by using the constrained transport technique (Evans & Hawley 1988; Ryu *et al.* 1998; Balsara & Spicer 1999; Gardiner & Stone 2005).

These codes are run on supercomputing resources at the Universitat de València (Tirant, Vives) or within the Spanish Supercomputing Network (Red Española de Supercomputación, RES). The parallelization used in both codes permits a three-dimensional splitting of the grid for distributed memory architectures. In this contribution, we present simulations which typically use 512–1024 cores and require >100 khr computing hours.

3. Applications

3.1. *The RHD simulations*

3.1.1. *Long-term evolution*

One line of our work has been aimed at understanding the evolution of powerful jets through the density/pressure profile of their host galaxies, and what role they play in heating the intergalactic medium. Our simulations were set up as an initial grid covering $\sim$100–200 kpc in the three-dimensional case (Perucho *et al.* 2019; Perucho, Martí & Quilis 2022) to $\sim$1 Mpc in two-dimensional simulations (Perucho, Quilis & Martí 2011; Perucho *et al.* 2014). The jets are injected as a boundary condition, with properties expected for

https://doi.org/10.1017/S0022377823000892 Published online by Cambridge University Press

jets at the injection point, typically 1 kpc from the central formation engine. The ambient density at this distance is $\sim 10^5\,\mathrm{m}^{-3}$, and it drops with distance following a profile derived from modelling X-ray observations of radio galaxy 3C 31 (Hardcastle *et al.* 2002).

At these scales, the jet is expected to be dominated by kinetic energy flux, and the magnetic field to have a dominant disordered component, thus only contributing to pressure, but triggering minor tension forces. This is an assumption that we apply to simulate these scenarios with RHD codes.

The jets are injected into the grid with a mildly relativistic velocity $0.9\,c$ and specific enthalpies around c^2. All these simulations show that collimated relativistic jets generate high-pressure regions of shocked jet gas. The high sound speed in this region facilitates equilibrium within the whole shocked region, feeding pressure-driven shock expansion. Altogether, this is a very efficient process in terms of energy transfer from the jet to the ambient medium, as explained in Perucho *et al.* (2017*b*). The main point that the simulations revealed is that, because the post-shock pressure depends on the momentum flux density, collimated relativistic jets transfer most of their energy flux (which is not dominated by the rest-mass energy of the particles, as happens in classical jets) to the ambient medium via shock heating.

Jet collimation is maintained due to its propagation through a decreasing density/pressure environment, which favours a faster decrease in the pressure of the shocked region, allowing (i) the jet to expand with small opening angles, and (ii) the increase of the relative value of jet-to-ambient inertia, which limits the growth rates of unstable modes (Hardee 1982). Furthermore, the jet advance velocity through such an ambient medium also increases with distance as compared with a homogeneous constant density jet. All these factors also contribute to a decrease of the growth rates of unstable modes (Perucho, Martí & Hanasz 2005; Perucho 2019), and to faster expansion, thus allowing the jet to develop to large scales while keeping its collimation.

In summary, our simulations have shown that powerful relativistic outflows ($L_j \geq 10^{38}\,\mathrm{W}$) propagating through galactic atmospheres are extremely efficient in heating the interstellar and intergalactic gas because of (i) their energy flux is not dominated by rest-mass energy of the particles, and (ii) they can keep their collimation.

Figures 1 and 2 show the results from two of the described simulations, with different ambient medium core densities: $10^{-7}\,\mathrm{m}^{-3}$ in the former and $4 \times 10^{-7}\,\mathrm{m}^{-3}$ in the latter (Perucho et al. 2019, 2022). The images show cuts of rest-mass density and pressure weighted with tracer and a rendering of jet mass fraction (tracer) that show the jet structure for the last snapshot of each simulation at times $\simeq 5.4\,\mathrm{Myr}$ and $\simeq 8\,\mathrm{Myr}$, respectively. In both cases, the jets generate thin backflow/cocoon regions, as caused by the fast propagation through the density decreasing galactic atmosphere. The increased ambient density triggers slightly inflated backflow regions around the jet's terminal shock.

Figure 3 shows projected pseudosynchrotron emissivity images (at viewing angles of 15°) of the three-dimensional RHD simulations displayed in figures 1 and 2, from a dynamical point of view. The expression used to compute the emissivity at a given frequency is the same as that used by Hardee (2003) (see also Clarke, Norman & Burns 1989)

$$\epsilon_\nu \propto n^{1-2\alpha} p^{2\alpha} (B \sin\theta_B)^{1+\alpha} D^{2+\alpha}, \tag{3.1}$$

where n is the particle number density, p is pressure, B is the assumed magnetic field strength, taken to be proportional to $\sqrt{p}$, θ_B is the angle between the field lines and the viewing angle assumed to be a constant, D is the Doppler factor and α is the spectral index (defined as $S_\nu \propto \nu^{-\alpha}$), taken as constant and equal to 0.5 (see, e.g. Heavens & Drury 1988; Kirk & Duffy 1999). This expression represents a raw approximation, with strong

https://doi.org/10.1017/S0022377823000892 Published online by Cambridge University Press

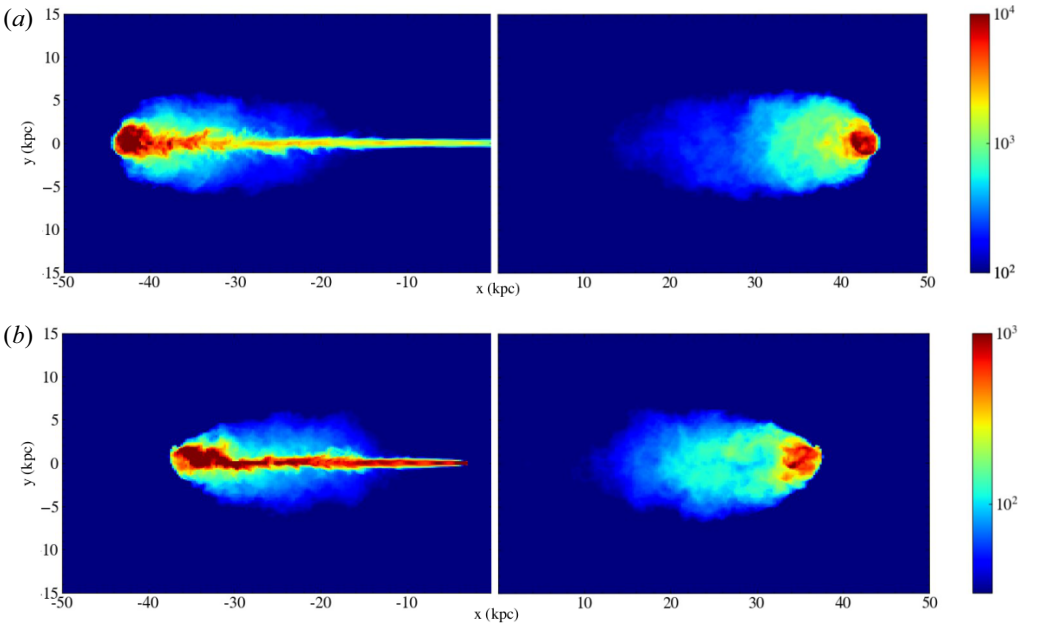

FIGURE 3. Pseudosynchrotron emissivity images of the jets shown in figures 1 (*a*) and 2 (*b*) computed with (3.1), in arbitrary units.

simplifications as that relative to the magnetic field structure or spectral indeces. This assumption cancels differences in emissivity caused by changes in θ_B, but this is expected to be a second-order contribution.[2] Therefore, the approach is enough to show relevant features. Furthermore, a detailed distribution of the magnetic field across the grid would require a fully RMHD simulation, which is left for future simulations of AGN jets (see § 3.2). The images show the effect of the Doppler factor in generating the jet-to-counter-jet brightness asymmetry and reproduce the canonical FRII jet morphology (see, e.g. Bridle 1984; Bridle & Perley 1984; Harwood *et al.* 2016), with emissivity enhancements at recollimation shocks, and bright hotspots surrounded by radio lobes.

3.1.2. *Mass load*

Less powerful jets ($L_j \leq 10^{36}$ W) can be decelerated by mass entrainment (Bicknell 1984). This process may take place in different ways, but mainly through the development of (Kelvin–Helmholtz, current driven, centrifugal…) instabilities at the jet boundary (e.g. Meliani & Keppens 2007; Perucho & Martí 2007; Matsumoto & Masada 2013; Massaglia *et al.* 2016, 2019, 2022; Matsumoto, Aloy & Perucho 2017; Gourgouliatos & Komissarov 2018) or by interactions between the jet and stars or clouds that cross it while orbiting the galactic centre (e.g. Komissarov (1994), Bowman, Leahy & Komissarov (1996), Laing & Bridle (2002), Hubbard & Blackman (2006), Perucho *et al.* (2014), Perucho (2019), Anglés-Castillo *et al.* (2021) and references therein).

Modelling of FRI jets has revealed that the region in which jets seem to become symmetric in brightness with respect to their counter-jets is also a region in which they become bright and that deceleration takes place progressively, from the jet boundaries towards their axes (Laing & Bridle 2014). This indicates that deceleration is driven by

[2]The field is expected to be mainly aligned with the jet in powerful outflows (e.g. Bridle 1984), perpendicular to the jet at the hotspot, randomly oriented in the lobes and aligned with the bow shock at the outermost surface.

https://doi.org/10.1017/S0022377823000892 Published online by Cambridge University Press

small-scale processes that take place at the boundaries and points towards either small wavelength instability modes arising at the shear transition with the jet environment or towards other kinds of perturbative interactions (Perucho *et al.* 2017*a*; Perucho 2020).

In the case of clouds and stars interacting with the jet, a bow shock is formed against the jet flow, and the mixing and loading process takes place at the cometary tail formed downstream of the interaction site (Komissarov 1994). It has been suggested that this process alone could decelerate low power jets ($L_j \leq 10^{35}$ W, Bowman *et al.* 1996; Perucho *et al.* 2014) and also change the properties (composition, magnetization...) in intermediate power jets ($L_j \sim 10^{36}$ W, Anglés-Castillo *et al.* 2021). These changes would be forced, according to Anglés-Castillo *et al.* (2021), by the relevant relative contribution of the rest-mass density of protons with respect to the jet's injected electron–positron pairs, on the one hand, and the corresponding increase in kinetic energy flux and gas pressure, which reduces the dynamical relevance of the magnetic field, on the other hand.

Furthermore, these interactions can host particle acceleration and generate the production of high-energy radiation and, altogether, may produce the brightness flaring in decelerating jets (e.g. Bednarek & Protheroe 1997; Bosch-Ramon, Perucho & Barkov 2012*b*; Wykes *et al.* 2013, 2015; Vieyro, Torres-Albà & Bosch-Ramon 2017; Torres-Albà & Bosch-Ramon 2019; Perucho 2020).

Numerical simulations have allowed us to characterize these scenarios and estimate the radiative output from them at different jet scales, e.g. parsecs and hundreds of parsecs (Bosch-Ramon *et al.* 2012*b*; Perucho *et al.* 2017*a*). Future work should be focused on understanding the role of magnetic fields in these collisions and the study of particle acceleration and cosmic ray production (e.g. Wykes *et al.* 2013; Murase, Oikonomou & Petropoulou 2018).

3.1.3. *Jet–ISM interactions*

Another aspect that has improved during the last decade in the field of AGN jet simulations is the characterization of galactic ambient media, both inside and outside the host galaxies (see, e.g. Wagner, Bicknell & Umemura 2012; Mukherjee *et al.* 2016; Bicknell *et al.* 2018; Mandal *et al.* 2021; Perucho *et al.* 2021). Galactic environments have started to be set up by using distributions obtained from cosmological simulations (e.g. Heinz *et al.* 2006; Yates-Jones, Shabala & Krause 2021). Within host galaxies, the two-phase nature of the ISM, with cold denser gas hosted in clouds and hot more dilute gas between them represents a non-negligible property to consider. This is especially relevant within the inner kiloparsec of host galaxies, where the broad and narrow line regions are located.

In addition, observational results at radio-to-UV ranges show that the jets trigger line emission and gas motions in their host galaxies (Morganti & Oosterloo 2018). Based on previous work by Vaidya *et al.* (2015), we have included hydrogen ionization and recombination feedback effects in our RHD code with the aim of tracing the effect of jets on the cold gas in the inner kiloparsec (Perucho *et al.* 2021). We have now improved the set up, using realistic ambient/cloud densities and temperatures. In these simulations, a purely leptonic (e^-/e^+) jet is injected into an inhomogeneous medium composed of a mixture of clouds that host atomic hydrogen, at temperatures $\sim$100 K and maximum density $n \sim 10^9\,\mathrm{m}^{-3}$, and an ionized medium with $T \sim 10^6$ K and $n \sim 10^5\,\mathrm{m}^{-3}$. The numerical box reproduces the inner 500 pc in the host galaxy, with the jet injected as a boundary condition at a certain distance from the forming region with relativistic velocity $0.98\,c$, density $\rho_j = 1.67 \times 10^{-26}\,\mathrm{kg\,m}^{-3}$ and a very high specific internal energy $\varepsilon \sim 10^3\,c^2$ to simulate the high pressure expected in this region (the simulation does not include a magnetic field so this approach could only account for a magnetic pressure generated by

https://doi.org/10.1017/S0022377823000892 Published online by Cambridge University Press

a disordered field configuration). In the simulations, the ambient medium is also given a transverse velocity of $100\,\mathrm{km\,s^{-1}}$ to emulate the rotation around the galactic nucleus.

Altogether, the parameter range in the simulations spans more than eight orders of magnitude in density and pressure, which makes the simulation extremely challenging. Moreover, time-step limiters need to be included to allow for the short hydrogen recombination rates in cold regions or ionization in shocked cells. The simulation uses two equations of state: a relativistic (Synge 1957) and a non-relativistic (see Vaidya *et al.* 2015) ideal gas. The criterion to choose between them in each cell is based on the composition, namely, on the fact that neutral hydrogen is present or not in the cell. The top panels of figure 4 show cuts of rest-mass density (left, in code units $\rho_a = 10^7\,\mathrm{m_p\,m^{-3}}$, with an upper limit to the colour scale set at $\rho_a = 10^8\,\mathrm{m_p\,m^{-3}}$), pressure (centre, in code units $\rho_a c^2 = 1.5 \times 10^{-3}$ Pa, with a lower limit set at $\rho_a c^2 = 1.5 \times 10^{-8}$ Pa) and velocity field (right, in code units c, limited at $10^{-5}\,c$) at the last snapshot obtained for the simulation, which is still being run, at $t = 460$ yr after injection. These plots reveal a complex shock structure around the jet as forced by the strong inhomogeneity in density found in the ambient medium. The shocked region is also highly inhomogeneous in density, revealing the richness in the interaction between the jet and the ISM shocked gas. The high sound speed contributes to homogenizing the pressure within the shocked region with the exception of some knots of denser (ambient) gas, and the jet's hotspot. Finally, the velocity field shows a wide range of values, from 10^{-4} to $0.1\,c$. Obviously, the smaller velocities correspond to the denser regions (see the comparison with the density panel). Although there are regions with values that can fall to several tens of km/s (blue colour within the shocked area, $\sim 10^{-4}\,c$), the dominating blue–white transition implies typical velocities of the order of hundreds to a thousand km/s. These values are in agreement with the typical ones measured from line emission in jetted active galaxies (see, e.g. Morganti & Oosterloo 2018; Schulz *et al.* 2021).

The bottom left panel in figure 4 shows a limited box centred on the region occupied by the jet structure with the rendering of a tracer that indicates the regions where originally dense cloud atomic gas can be found. From the image, it is evident that this gas is fixed in clouds outside the shocked volume, but it is completely disrupted and mixed by the shock, and appears concentrated towards the shock region. Finally, the bottom right panel displays, for the same box, a collection of isosurfaces of pressure (red) to highlight the shock wave (red, $7 \times 10^{-7}\rho_a c^2 \simeq 10^{-10}$ Pa), leptonic number (dark blue, $\rho_{e^-/e^+}/\rho$ at 10^{-3}, as compared with $\simeq 5.4 \times 10^{-4}$ for e^-/p gas) to show the jet and still lepton dominated unmixed regions, atomic hydrogen density outside the shock (orange, for $10^8\,\mathrm{m_p\,m^{-3}}$) to show the cloud distribution and inside the shock (bluish, for $10^5\,\mathrm{m_p\,m^{-3}}$) to show hints of atomic hydrogen within the shocked cavity. The low density (bluish) hydrogen density contours follow clearly the shock surface and thus reveal a very fast and complete ionization of the atomic gas. Therefore, we observe that the shocked gas is completely ionized, so despite our simulation recovering the observed velocities, as stated above, it also shows that the shocks produced by powerful jets ionize atomic (and therefore molecular) gas very rapidly and this forbids line detection, unlike what the observations clearly reveal. The origin of this discrepancy probably lies in the fact that observed lines correspond to radio sources more evolved than our simulation at the current position (several kpc vs 200 pc) and that post-shock temperatures (typically 10^6–10^7 K) are too high to allow for recombination of shock-ionized hydrogen within the simulated time. Nevertheless, we observe white spotted areas in the cuts (top left panel) which imply densities between 10^7 and $10^8\,\mathrm{m_p\,m^{-3}}$ and this could translate in cooling times of $\sim 10^{3-4}$–10^{4-5} yr for gas between solar and 0 metallicity at the aforementioned temperatures (Dopita & Sutherland 2003). Although the simulations are limited to pairs,

https://doi.org/10.1017/S0022377823000892 Published online by Cambridge University Press

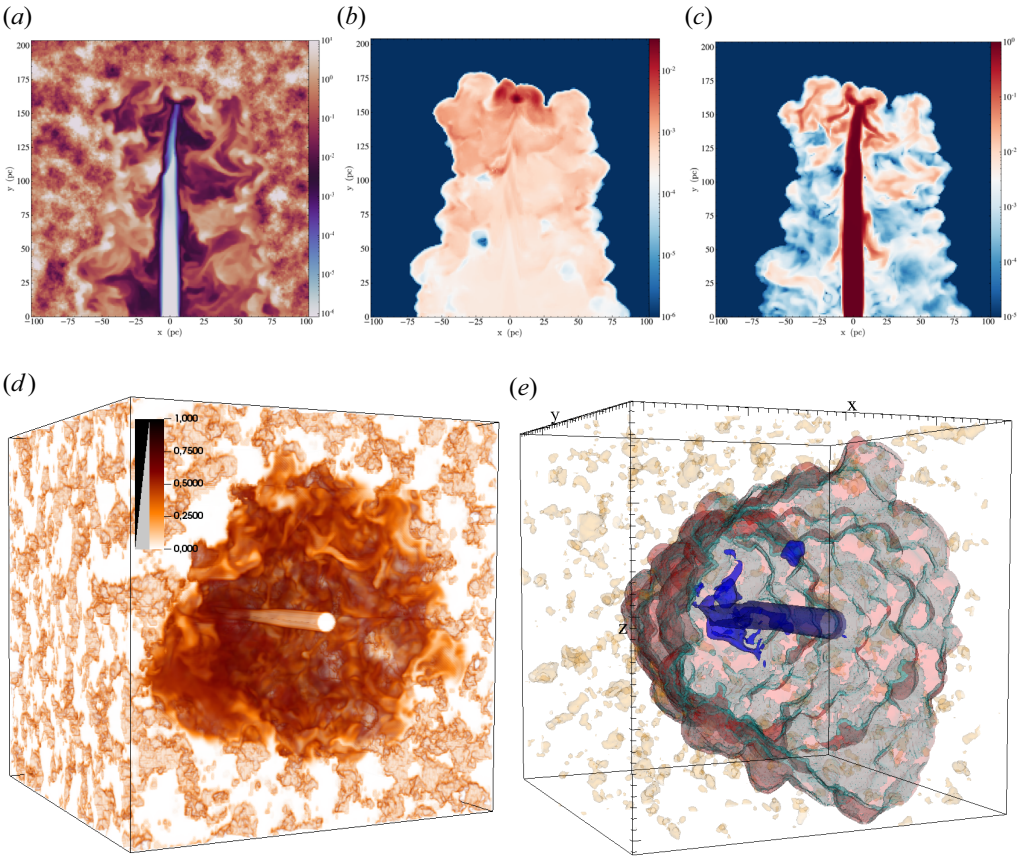

FIGURE 4. (*a–c*) Cuts of rest-mass density ((*a*), in code units $\rho_a = 10^7\,\mathrm{m_p\,m^{-3}}$), pressure ((*b*), in code units $\rho_a c^2 = 1.5 \times 10^{-3}$ Pa) and velocity field ((*c*), in code units *c*) at $t = 460$ yr after injection. (*d*) Tracer rendering showing the locations with originally dense, cloud, atomic gas (left). (*e*) isosurfaces of pressure (red, $\simeq 10^{-10}$ Pa), leptonic number (dark blue, $\rho_{e^-/e^+}/\rho = 10^{-3}$), atomic hydrogen density outside the shock (orange, $10^8\,\mathrm{m_p\,m^{-3}}$) and inside the shock (bluish, $10^5\,\mathrm{m_p\,m^{-3}}$).

and atomic+ionized hydrogen in the composition of the gas, they show that the conditions for line emission with the observed velocities could be recovered once the jet has evolved for at least twice the simulated time so far. Therefore our simulations represent a promising first step in the understanding of the ISM dynamics driven by jet injection in the host galaxies.

3.2. *The RMHD simulations*

3.2.1. *Jet–stellar wind interactions*

Jets in X-ray binaries propagate through the binary environment before carving their way towards the ISM. In this region, especially in the case of massive binaries, jets travel through a dense, slow stellar wind that can produce a strong lateral impact on the jet flow, triggering internal shocks and, in the case of low power jets, even disruption. This was proposed as a plausible scenario for triggering gamma-ray radiation and thus explaining the emission physics of the very few gamma-ray emitting binaries observed in the Galaxy

https://doi.org/10.1017/S0022377823000892 Published online by Cambridge University Press

(see e.g. Rieger, Bosch-Ramon & Duffy 2007; Bosch-Ramon & Khangulyan 2009*b* and references therein).

Following a number of papers that studied RHD simulations of jet–massive wind interactions (Perucho & Bosch-Ramon 2008; Perucho *et al.* 2010*a*; Perucho & Bosch-Ramon 2012), we run a set of dedicated three-dimensional numerical simulations using our new code LÓSTREGO, including the dynamical effects of magnetic fields (López-Miralles *et al.* 2022). The results of these simulations showed that the latter could play a stabilizing role – and thus, to provide extra collimation within the binary scale – in the jet evolution when the flux of magnetic energy is low compared with the flux of kinetic energy, while a non-negligible magnetic energy flux makes the jet prone to the development of current-driven instabilities within the scale of the binary.

The dynamics of the jet model with a dynamically relevant field in López-Miralles *et al.* (2022) is particularly interesting from several points of view. The jet evolution during the interaction with the stellar wind is significantly different with respect to a hydrodynamical jet with the same total power: whereas a powerful hydrodynamical jet evolves without losing collimation, the magnetized jet is prone to the development of current-driven instability pinching and kink modes triggered by overpressure and the toroidal field. Therefore, the jet shows a chain of recollimation shocks within the binary scale, followed by the development of a strong kink that spreads the jet momentum throughout a large area and decelerates its advance. The magnetic field structure is toroidal from injection to the development of the kink, while it becomes highly entangled near the head, filling the cavity.

In figure 5 we present the resulting configuration of the magnetic field in this simulation by focusing on the field lines. This plot shows relevant information about the field structure in the jet spine, which was hidden by the mixed plasma in the cocoon in our representation in López-Miralles *et al.* (2022). Since the magnetic field within the cocoon is low compared with that in the jet, we have applied a linear transparency to the field lines, weighted by the field vector module. In the mid–low part of the jet, the magnetic field preserves the toroidal structure of injection, which is reinforced at the recollimation shocks, as expected. The jet tracer three-dimensional render (top panel), which is limited to $f > 0.9$ to highlight the jet core, shows a pinched morphology and a set of annuli of jet plasma surrounding the core, which are deposited in the cavity due to the jet dynamics during the first stages of propagation. This morphology is very particular and could give rise to different emission patterns that deserve to be studied in detail, but this is out of the scope of this contribution. In the mid–upper part of the simulation, both the new representation of the field and the tracer function allow us to distinguish a well-resolved precessing morphology, triggered by the development of a kink instability. The inset plot of figure 5 zooms in on the jet head, showing that the field is highly reinforced at the elbow of the twisted trace, which is also directly impacting the shocked environment formed by the stellar wind.

Further analysis will be required to investigate the consequences of this precessing morphology on the jet dynamics (within and beyond the binary), on the one hand, and its implications in terms of non-thermal emission, on the other. This kink could contribute to the observed signatures of precessing jets that have been resolved at radio wavelengths for different X-ray binaries with jet-like structures. The most relevant example of jet precession is the well-known microquasar SS 433, but there are many other examples (see e.g. Mioduszewski *et al.* 2001; Massi, Ros & Zimmermann 2012; Miller-Jones *et al.* 2019; Luque-Escamilla, Martí & Martínez-Aroza 2020). The origin of precession in microquasars is still debated for most of these sources. Although the classical theoretical models tend to explain precession by invoking relativistic effects of

https://doi.org/10.1017/S0022377823000892 Published online by Cambridge University Press

(*a*)

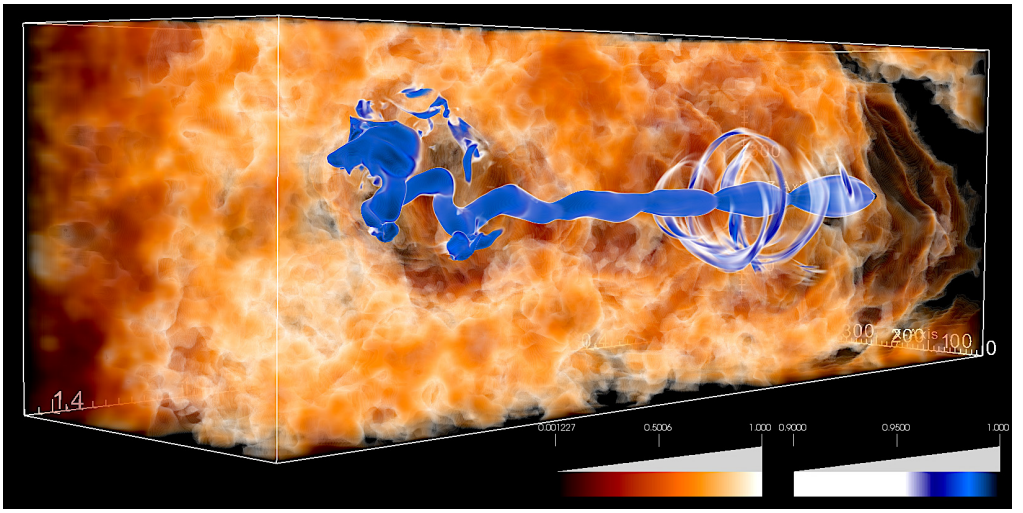

(*b*)

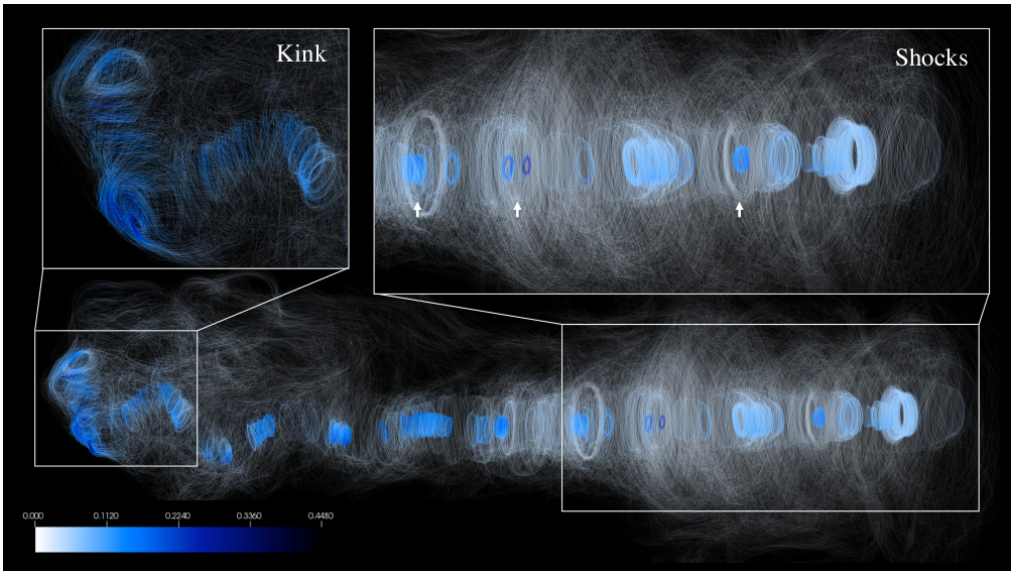

FIGURE 5. (*a*) Three-dimensional rendering visualization of the jet core ($f > 0.9$) propagating through the clumpy stellar wind. (*b*) Magnetic field lines integrated in the three-dimensional volume, where the colour map represents the magnetic field vector module. The transparency of the lines is inversely proportional to the vector module to highlight the jet skeleton. Inset plots zoomed in the recollimation shock region (right) and the twisted trace triggered by the kink instability (left).

the inner disc (i.e. Lense–Thirring precession, Liska *et al.* 2018; Motta *et al.* 2018) or the coupled effect of stellar winds and orbital motion (Barkov & Bosch-Ramon 2022), our simulation shows that current-driven instabilities can also trigger helical patterns during the jet–wind interaction, although the periods associated with this kind of precession should be accurately related. For example, current-driven instabilities have been claimed

https://doi.org/10.1017/S0022377823000892 Published online by Cambridge University Press

to explain the large-scale morphology of the jet structures observed in GRS 1758-258 (Luque-Escamilla *et al.* 2020).

This simulated jet thus represents an extraordinary candidate to produce high-energy radiation in microquasars, since energy dissipation may not only occur at the several reconfinement shocks where particles can be accelerated, but also a kink instability that can lead to kink-driven magnetic reconnection processes further out from the injection base (see e.g. Bodo, Tavecchio & Sironi 2021; Bodo *et al.* 2022). The characterization of the periodic behaviour of these processes (i.e. shocks and kink-driven precession) can be also relevant to interpreting the rapid X-ray variability of some X-ray binaries/microquasars. Therefore, future work will include consideration of those dissipative processes in the acceleration of non-thermal particles and the triggering of high-energy radiative output. Although magnetic reconnection is not reproduced in ideal RMHD codes like ours, recipes such as those presented in Bodo *et al.* (2021) will allow us to characterize the formation of current sheets and magnetic dissipation regions into our simulation. We expect that the combination of such analysis with numerical simulations such as those presented in this contribution, will provide new insights into the physical processes that lead to non-thermal emission in microquasars jets within the scale of the binary.

4. Conclusions

In this paper, we have presented a number of scenarios that require the use of numerical codes to study due to their extreme nature, which makes this research prohibitive for current laboratory experimental capabilities. All these scenarios have in common the need for relativistic (magneto-)hydrodynamics, and they use similar methods to solve the system of equations that is used to model them. Different improvements have been made in the codes used in our group through the past years, including optimization and parallelization, modelling of ambient media, etc. These improvements have allowed us to tackle more realistic simulations, which, although still far from reproducing the studied scenarios accurately, have brought about relevant advances in our knowledge of the physics of relativistic outflows in astrophysics and their impact on their environment. Future work should address in detail the role of magnetic fields in the evolution and impact of jets in the scenarios previously studied with RHD simulations while, at the same time, improving the physical processes that the codes take into account and that can be relevant for studying those scenarios. One such improvement consists of including the radiation dynamics, which could allow us to compare the role of shocks and radiative output from the central engines (accretion disks) in shaping the heating mechanisms of the ISM and the intergalactic medium (IGM/WHIM). Future improvements of codes will be related to linking multi-scale processes and adding relevant physics to improve the simulations of astrophysical scenarios that are still extremely challenging for current supercomputing capabilities and far from realistic for laboratory experiments.

Acknowledgements

M.P. acknowledges M. Perucho-Franco, his father, for standing up as an example through his whole life. The authors thank the referees for their constructive comments.

Editor Luís O. Silva thanks the referees for their advice in evaluating this article.

Funding

Computer simulations have been carried out in the Servei d'Informàtica de la Universitat de València (Tirant). This work has been supported by the Spanish Ministry of

Science through Grants PID2019-105510GB-C31/AEI/10.13039/501100011033, PID2019-107427GB-C33, from the Generalitat Valenciana through grant PROMETEU/2019/071, it was also funded by the Deutsche Forschungsgemeinschaft (DFG, German Research Foundation) – project number 443220636, and it forms part of the Astrophysics and High Energy Physics programme and was supported by MCIN with funding from European Union NextGenerationEU (PRTR-C17.I1) and by Generalitat.

Declaration of interests

The authors report no conflict of interest.

Author contributions

Both authors contributed to analysing data and reaching conclusions, and in writing the paper.

REFERENCES

ANGLÉS-CASTILLO, A., PERUCHO, M., MARTÍ, J.M. & LAING, R.A. 2021 On the deceleration of Fanaroff-Riley Class I jets: mass loading of magnetized jets by stellar winds. *Mon. Not. R. Astron. Soc*. **500** (1), 1512–1530.

BALSARA, D.S. & SPICER, D.S. 1999 A staggered mesh algorithm using high order Godunov fluxes to ensure solenoidal magnetic fields in magnetohydrodynamic simulations. *J. Comput. Phys*. **149** (2), 270–292.

BARKOV, M.V. & BOSCH-RAMON, V. 2022 Relativistic hydrodynamical simulations of the effects of the stellar wind and the orbit on high-mass microquasar jets. *Mon. Not. R. Astron. Soc*. **510** (3), 3479–3494.

BEDNAREK, W. & PROTHEROE, R.J. 1997 Gamma-rays from interactions of stars with active galactic nucleus jets. *Mon. Not. R. Astron. Soc*. **287** (3), L9–L13.

BELLAN, P.M. 2018 Experiments relevant to astrophysical jets. *J. Plasma Phys*. **84** (5), 755840501.

BICKNELL, G.V. 1984 A model for the surface brightness of a turbulent low Mach number jet. I. Theoretical development and application to 3C 31. *Astrophys. J*. **286**, 68–87.

BICKNELL, G.V., MUKHERJEE, D., WAGNER, A.Y., SUTHERLAND, R.S. & NESVADBA, N.P.H. 2018 Relativistic jet feedback - II. Relationship to gigahertz peak spectrum and compact steep spectrum radio galaxies. *Mon. Not. R. Astron. Soc*. **475** (3), 3493–3501.

BLANDFORD, R.D. & PAYNE, D.G. 1982 Hydromagnetic flows from accretion disks and the production of radio jets. *Mon. Not. R. Astron. Soc*. **199**, 883–903.

BLANDFORD, R.D. & REES, M.J. 1974 A 'twin-exhaust' model for double radio sources. *Mon. Not. R. Astron. Soc*. **169**, 395–415.

BLANDFORD, R.D. & ZNAJEK, R.L. 1977 Electromagnetic extraction of energy from Kerr black holes. *Mon. Not. R. Astron. Soc*. **179**, 433–456.

BODO, G., MAMATSASHVILI, G., ROSSI, P. & MIGNONE, A. 2022 Current-driven kink instabilities in relativistic jets: dissipation properties. *Mon. Not. R. Astron. Soc*. **510** (2), 2391–2406.

BODO, G., TAVECCHIO, F. & SIRONI, L. 2021 Kink-driven magnetic reconnection in relativistic jets: consequences for X-ray polarimetry of BL Lacs. *Mon. Not. R. Astron. Soc*. **501** (2), 2836–2847.

BORDAS, P., BOSCH-RAMON, V., PAREDES, J.M. & PERUCHO, M. 2009 Non-thermal emission from microquasar/ISM interaction. *Astron. Astrophys*. **497** (2), 325–334.

BOSCH-RAMON, V., BARKOV, M.V., KHANGULYAN, D. & PERUCHO, M. 2012*a* Simulations of stellar/pulsar-wind interaction along one full orbit. *Astron. Astrophys*. **544**, A59.

BOSCH-RAMON, V., BARKOV, M.V. & PERUCHO, M. 2015 Orbital evolution of colliding star and pulsar winds in 2D and 3D: effects of dimensionality, EoS, resolution, and grid size. *Astron. Astrophys*. **577**, A89.

BOSCH-RAMON, V. & KHANGULYAN, D. 2009*a* Understanding the very-high emission from microquasars. *Intl J. Mod. Phys.* D **18** (3), 347–387.

Bosch-Ramon, V. & Khangulyan, D. 2009*b* Understanding the very-high emission from microquasars. *Intl J. Mod. Phys.* D **18** (3), 347–387.

Bosch-Ramon, V., Perucho, M. & Barkov, M.V. 2012*b* Clouds and red giants interacting with the base of AGN jets. *Astron. Astrophys*. **539**, A69.

Bowman, M., Leahy, J.P. & Komissarov, S.S. 1996 The deceleration of relativistic jets by entrainment. *Mon. Not. R. Astron. Soc*. **279**, 899.

Bridle, A.H. 1984 Sidedness, field configuration, and collimation of extragalactic radio jets. *Astron. J*. **89**, 979–986.

Bridle, A.H. & Perley, R.A. 1984 Extragalactic radio jets. *Annu. Rev. Astron. Astrophys*. **22**, 319–358.

Buson, S., Tramacere, A., Oswald, L., Barbano, E., Fichet de Clairfontaine, G., Pfeiffer, L., Azzollini, A., Baghmanyan, V. & Ajello, M. 2023 Extragalactic neutrino factories. arXiv:2305.11263.

Charlet, A., Walder, R., Marcowith, A., Folini, D., Favre, J.M. & Dieckmann, M.E. 2022 Effects of radiative losses on the relativistic jets of high-mass microquasars. *Astron. Astrophys*. **658**, A100.

Clarke, D.A., Norman, M.L. & Burns, J.O. 1989 Numerical observations of a simulated jet with a passive helical magnetic field. *Astrophys. J*. **342**, 700.

Croston, J.H., Hardcastle, M.J., Mingo, B., Best, P.N., Sabater, J., Shimwell, T.M., Williams, W.L., Duncan, K.J., Röttgering, H.J.A., Brienza, M., *et al.* 2019 The environments of radio-loud AGN from the LOFAR Two-Metre Sky Survey (LoTSS). *Astron. Astrophys*. **622**, A10.

de la Cita, V.M., Bosch-Ramon, V., Paredes-Fortuny, X., Khangulyan, D. & Perucho, M. 2017 Non-thermal radiation from a pulsar wind interacting with an inhomogeneous stellar wind. *Astron. Astrophys*. **598**, A13.

Dopita, M.A. & Sutherland, R.S. 2003 *Astrophysics of the diffuse universe.* A&A Library. ISSN 0941-7834. Berlin, Heidelberg, New York:Springer.

Evans, C.R. & Hawley, J.F. 1988 Simulation of magnetohydrodynamic flows: a constrained transport model. *Astrophys. J*. **332**, 659.

Fabian, A.C. 2012 Observational evidence of active galactic nuclei feedback. *Annu. Rev. Astron. Astrophys*. **50**, 455–489.

Fanaroff, B.L. & Riley, J.M. 1974 The morphology of extragalactic radio sources of high and low luminosity. *Mon. Not. R. Astron. Soc*. **167**, 31P–36P.

Fender, R. 2006 Jets from X-ray binaries. In *Compact stellar X-ray sources*, (eds. Walter Lewin & Michiel van der Klis), Cambridge Astrophysics Series, vol. 39. Cambridge, UK: Cambridge Cambridge University Press, pp. 381–419. ISBN 978-0-521-82659-4, ISBN 0-521-82659-4, doi: 10.2277/0521826594.

Fender, R.P., Belloni, T.M. & Gallo, E. 2004 Towards a unified model for black hole X-ray binary jets. *Mon. Not. R. Astron. Soc*. **355** (4), 1105–1118.

Gardiner, T.A. & Stone, J.M. 2005 An unsplit Godunov method for ideal MHD via constrained transport. *J. Comput. Phys*. **205** (2), 509–539.

Gourgouliatos, K.N. & Komissarov, S.S. 2018 Reconfinement and loss of stability in jets from active galactic nuclei. *Nat. Astron*. **2**, 167–171.

Hardcastle, M.J., Worrall, D.M., Birkinshaw, M., Laing, R.A. & Bridle, A.H. 2002 A Chandra observation of the X-ray environment and jet of 3C 31. *Mon. Not. R. Astron. Soc*. **334** (1), 182–192.

Hardee, P.E. 1982 Helical and pinching instability of supersonic expanding jets in extragalactic radio sources. *Astrophys. J*. **257**, 509–526.

Hardee, P.E. 2003 Modeling helical structures in relativistic jets. *Astrophys. J*. **597** (2), 798–808.

Harten, A., Lax, P. & van Leer, B. 1983 On upstream differencing and Godunov-type schemes for hyperbolic conservation laws. *SIAM Rev*. **25**, 35–61.

Harwood, J.J., Croston, J.H., Intema, H.T., Stewart, A.J., Ineson, J., Hardcastle, M.J., Godfrey, L., Best, P., Brienza, M., Heesen, V., *et al.* 2016 FR II radio galaxies at low frequencies - I. Morphology, magnetic field strength and energetics. *Mon. Not. R. Astron. Soc*. **458** (4), 4443–4455.

HEAVENS, A.F. & DRURY, L.O.C. 1988 Relativistic shocks and particle acceleration. *Mon. Not. R. Astron. Soc*. **235**, 997–1009.

HEINZ, S., BRÜGGEN, M., YOUNG, A. & LEVESQUE, E. 2006 The answer is blowing in the wind: simulating the interaction of jets with dynamic cluster atmospheres. *Mon. Not. R. Astron. Soc*. **373** (1), L65–L69.

HUBBARD, A. & BLACKMAN, E.G. 2006 Active galactic nuclei jet mass loading and truncation by stellar winds. *Mon. Not. R. Astron. Soc*. **371** (4), 1717–1721.

ICKE, V. 1991 From nucleus to hotspot: nine powers of ten. In *Beams and Jets in Astrophysics*, (eds. P.A. Hughes), Cambridge Astrophysics Series, vol. 19. Cambridge, UK: Cambridge University Press, p. 232.

KIRK, J.G. & DUFFY, P. 1999 TOPICAL REVIEW: particle acceleration and relativistic shocks. *J. Phys.* G **25** (8), R163–R194.

KOMISSAROV, S. 2012 Central engines: acceleration, collimation and confinement of jets. In *Relativistic Jets from Active Galactic Nuclei*, (eds. M. Boettcher, D.E. Harris & H. Krawczynski), Berlin: Wiley, pp. 81–114.

KOMISSAROV, S.S. 1994 Mass-loaded relativistic jets. *Mon. Not. R. Astron. Soc*. **269**, 394.

KOMISSAROV, S.S. 1999 A Godunov-type scheme for relativistic magnetohydrodynamics. *Mon. Not. R. Astron. Soc*. **303** (2), 343–366.

KOMISSAROV, S.S., BARKOV, M.V., VLAHAKIS, N. & KÖNIGL, A. 2007 Magnetic acceleration of relativistic active galactic nucleus jets. *Mon. Not. R. Astron. Soc*. **380** (1), 51–70.

LAING, R.A. & BRIDLE, A.H. 2002 Dynamical models for jet deceleration in the radio galaxy 3C 31. *Mon. Not. R. Astron. Soc*. **336** (4), 1161–1180.

LAING, R.A. & BRIDLE, A.H. 2014 Systematic properties of decelerating relativistic jets in low-luminosity radio galaxies. *Mon. Not. R. Astron. Soc*. **437** (4), 3405–3441.

LISKA, M., HESP, C., TCHEKHOVSKOY, A., INGRAM, A., VAN DER KLIS, M. & MARKOFF, S. 2018 Formation of precessing jets by tilted black hole discs in 3D general relativistic MHD simulations. *Mon. Not. R. Astron. Soc*. **474** (1), L81–L85.

LÓPEZ-MIRALLES, J., MARTÍ, J.M. & PERUCHO, M. 2023 On the application of Jacobian-free Riemann solvers for relativistic radiation magnetohydrodynamics under M1 closure. *Comput. Phys. Commun*. **284**, 108630.

LÓPEZ-MIRALLES, J., PERUCHO, M., MARTÍ, J.M., MIGLIARI, S. & BOSCH-RAMON, V. 2022 3D RMHD simulations of jet-wind interactions in high-mass X-ray binaries. *Astron. Astrophys*. **661**, A117.

LUQUE-ESCAMILLA, P.L., MARTÍ, J. & MARTÍNEZ-AROZA, J. 2020 Effects of precession versus instabilities on the jets of GRS 1758-258. *Astron. Astrophys*. **643**, A150.

MANDAL, A., MUKHERJEE, D., FEDERRATH, C., NESVADBA, N.P.H., BICKNELL, G.V., WAGNER, A.Y. & MEENAKSHI, M. 2021 Impact of relativistic jets on the star formation rate: a turbulence-regulated framework. *Mon. Not. R. Astron. Soc*. **508** (4), 4738–4757.

MARTÍ, J.-M. 2019 Numerical simulations of jets from active galactic nuclei. *Galaxies* **7** (1), 24.

MARTÍ, J.M. & MÜLLER, E. 2015 Grid-based methods in relativistic hydrodynamics and magnetohydrodynamics. *Living Rev. Comput. Astrophys*. **1** (1), 3.

MASSAGLIA, S., BODO, G., ROSSI, P., CAPETTI, A. & MIGNONE, A. 2022 Making Fanaroff-Riley I radio sources. III. The effects of the magnetic field on relativistic jets' propagation and source morphologies. *Astron. Astrophys*. **659**, A139.

MASSAGLIA, S., BODO, G., ROSSI, P., CAPETTI, S. & MIGNONE, A. 2016 Making Faranoff-Riley I radio sources. I. Numerical hydrodynamic 3D simulations of low-power jets. *Astron. Astrophys*. **596**, A12.

MASSAGLIA, S., BODO, G., ROSSI, P., CAPETTI, S. & MIGNONE, A. 2019 Making Faranoff-Riley I radio sources. II. The effects of jet magnetization. *Astron. Astrophys*. **621**, A132.

MASSI, M., ROS, E. & ZIMMERMANN, L. 2012 VLBA images of the precessing jet of LS I $+61^{\circ}303$. *Astron. Astrophys*. **540**, A142.

MATSUMOTO, J., ALOY, M.A. & PERUCHO, M. 2017 Linear theory of the Rayleigh-Taylor instability at a discontinuous surface of a relativistic flow. *Mon. Not. R. Astron. Soc*. **472** (2), 1421–1431.

MATSUMOTO, J. & MASADA, Y. 2013 Two-dimensional numerical study for Rayleigh-Taylor and Richtmyer-Meshkov instabilities in relativistic jets. *Astrophys. J. Lett*. **772** (1), L1.

MATTHEWS, J.H., BELL, A.R. & BLUNDELL, K.M. 2020 Particle acceleration in astrophysical jets. *New Astron. Rev*. **89**, 101543.

MCNAMARA, B.R. & NULSEN, P.E.J. 2007 Heating hot atmospheres with active galactic nuclei. *Annu. Rev. Astron. Astrophys*. **45** (1), 117–175.

MELI, A. & NISHIKAWA, K.-I. 2021 Particle-in-cell simulations of astrophysical relativistic jets. *Universe* **7** (11), 450.

MELIANI, Z. & KEPPENS, R. 2007 Transverse stability of relativistic two-component jets. *Astron. Astrophys*. **475** (3), 785–789.

MIGLIARI, S., FENDER, R. & MÉNDEZ, M. 2002 Iron emission lines from extended X-ray jets in SS 433: reheating of atomic nuclei. *Science* **297** (5587), 1673–1676.

MIGNONE, A. & BODO, G. 2006 An HLLC Riemann solver for relativistic flows – II. Magnetohydrodynamics. *Mon. Not. R. Astron. Soc*. **368** (3), 1040–1054.

MIGNONE, A., UGLIANO, M. & BODO, G. 2009 A five-wave Harten–Lax–van Leer Riemann solver for relativistic magnetohydrodynamics. *Mon. Not. R. Astron. Soc*. **393** (4), 1141–1156.

MILLER-JONES, J.C.A., TETARENKO, A.J., SIVAKOFF, G.R., MIDDLETON, M.J., ALTAMIRANO, D., ANDERSON, G.E., BELLONI, T.M., FENDER, R.P., JONKER, P.G., KÖRDING, E.G., *et al.* 2019 A rapidly changing jet orientation in the stellar-mass black-hole system V404 Cygni. *Nature* **569** (7756), 374–377.

MIODUSZEWSKI, A.J., RUPEN, M.P., HJELLMING, R.M., POOLEY, G.G. & WALTMAN, E.B. 2001 A one-sided highly relativistic jet from Cygnus X-3. *Astrophys. J*. **553** (2), 766–775.

MIRABEL, I.F. 2010 Microquasars: summary and outlook. In *Lecture Notes in Physics* (ed. T. Belloni), vol. 794, p. 1. Springer.

MOLINA, M., BASSANI, L., MALIZIA, A., BIRD, A.J., BAZZANO, A., UBERTINI, P. & VENTURI, T. 2014 IGR J17488-2338: a newly discovered giant radio galaxy. *Astron. Astrophys*. **565**, A2.

MONCEAU-BAROUX, R., PORTH, O., MELIANI, Z. & KEPPENS, R. 2015 The SS433 jet from subparsec to parsec scales. *Astron. Astrophys*. **574**, A143.

MORGANTI, R. & OOSTERLOO, T. 2018 The interstellar and circumnuclear medium of active nuclei traced by H i 21 cm absorption. *Astron. Astrophys. Rev*. **26** (1), 4.

MOTTA, S.E., FRANCHINI, A., LODATO, G. & MASTROSERIO, G. 2018 On the different flavours of Lense-Thirring precession around accreting stellar mass black holes. *Mon. Not. R. Astron. Soc*. **473** (1), 431–439.

MUKHERJEE, D., BICKNELL, G.V., SUTHERLAND, R. & WAGNER, A. 2016 Relativistic jet feedback in high-redshift galaxies - I. Dynamics. *Mon. Not. R. Astron. Soc*. **461** (1), 967–983.

MURASE, K., OIKONOMOU, F. & PETROPOULOU, M. 2018 Blazar flares as an origin of high-energy cosmic neutrinos? *Astrophys. J*. **865** (2), 124.

MURASE, K. & STECKER, F.W. 2022 High-energy neutrinos from active galactic nuclei. arXiv:2202.03381.

OEI, M.S.S.L., VAN WEEREN, R.J., HARDCASTLE, M.J., BOTTEON, A., SHIMWELL, T.W., DABHADE, P., GAST, A.R.D.J.G.I.B., RÖTTGERING, H.J.A., BRÜGGEN, M., TASSE, C., *et al.* 2022 The discovery of a radio galaxy of at least 5 Mpc. *Astron. Astrophys*. **660**, A2.

PAREDES-FORTUNY, X., BOSCH-RAMON, V., PERUCHO, M. & RIBÓ, M. 2015 Simulations of an inhomogeneous stellar wind interacting with a pulsar wind in a binary system. *Astron. Astrophys*. **574**, A77.

PERUCHO, M. 2019 Dissipative processes and their role in the evolution of radio galaxies. *Galaxies* **7** (3), 70.

PERUCHO, M. 2020 Triggering mixing and deceleration in FRI jets: a solution. *Mon. Not. R. Astron. Soc*. **494** (1), L22–L26.

PERUCHO, M. & BOSCH-RAMON, V. 2008 On the interaction of microquasar jets with stellar winds. *Astron. Astrophys*. **482** (3), 917–927.

PERUCHO, M. & BOSCH-RAMON, V. 2012 3D simulations of microquasar jets in clumpy stellar winds. *Astron. Astrophys*. **539**, A57.

PERUCHO, M., BOSCH-RAMON, V. & BARKOV, M.V. 2017*a* Impact of red giant/AGB winds on active galactic nucleus jet propagation. *Astron. Astrophys*. **606**, A40.

PERUCHO, M., BOSCH-RAMON, V. & KHANGULYAN, D. 2010*a* 3D simulations of wind-jet interaction in massive X-ray binaries. *Astron. Astrophys*. **512**, L4.

PERUCHO, M., LÓPEZ-MIRALLES, J., REYNALDI, V. & LABIANO, Á. 2021 Jet propagation through inhomogeneous media and shock ionization. *Astron. Nachr*. **342** (1171), 1171–1175.

PERUCHO, M., MARTÍ, J.-M. & QUILIS, V. 2019 Long-term FRII jet evolution: clues from three-dimensional simulations. *Mon. Not. R. Astron. Soc*. **482** (3), 3718–3735.

PERUCHO, M., MARTÍ, J.-M. & QUILIS, V. 2022 Long-term FRII jet evolution in dense environments. *Mon. Not. R. Astron. Soc*. **510** (2), 2084–2096.

PERUCHO, M., MARTÍ, J.-M., QUILIS, V. & BORJA-LLORET, M. 2017*b* Radio mode feedback: does relativity matter? *Mon. Not. R. Astron. Soc*. **471** (1), L120–L124.

PERUCHO, M. & MARTÍ, J.M. 2007 A numerical simulation of the evolution and fate of a Fanaroff-Riley type I jet. The case of 3C 31. *Mon. Not. R. Astron. Soc*. **382** (2), 526–542.

PERUCHO, M., MARTÍ, J.M., CELA, J.M., HANASZ, M., DE LA CRUZ, R. & RUBIO, F. 2010*b* Stability of three-dimensional relativistic jets: implications for jet collimation. *Astron. Astrophys*. **519**, A41.

PERUCHO, M., MARTÍ, J.M. & HANASZ, M. 2005 Nonlinear stability of relativistic sheared planar jets. *Astron. Astrophys*. **443** (3), 863–881.

PERUCHO, M., MARTÍ, J.M., LAING, R.A. & HARDEE, P.E. 2014 On the deceleration of Fanaroff-Riley Class I jets: mass loading by stellar winds. *Mon. Not. R. Astron. Soc*. **441** (2), 1488–1503.

PERUCHO, M., QUILIS, V. & MARTÍ, J.-M. 2011 Intracluster medium reheating by relativistic jets. *Astrophys. J*. **743** (1), 42.

RIEGER, F. & LEVINSON, A. 2018 Radio galaxies at VHE energies. *Galaxies* **6** (4), 116.

RIEGER, F.M., BOSCH-RAMON, V. & DUFFY, P. 2007 Fermi acceleration in astrophysical jets. *Astrophys. Space Sci*. **309** (1–4), 119–125.

ROE, P.L. 1986 Discrete models for the numerical analysis of time-dependent multidimensional gas dynamics. *J. Comput. Phys*. **63** (2), 458–476.

RYU, D., MINIATI, F., JONES, T.W. & FRANK, A. 1998 A divergence-free upwind code for multidimensional magnetohydrodynamic flows. *Astrophys. J*. **509** (1), 244–255.

SCHULZ, R., MORGANTI, R., NYLAND, K., PARAGI, Z., MAHONY, E.K. & OOSTERLOO, T. 2021 Parsec-scale HI outflows in powerful radio galaxies. *Astron. Astrophys*. **647**, A63.

SEO, J., RYU, D. & KANG, H. 2022 A simulation study of ultra-relativistic jets – III. Particle acceleration at FR-II jets. arXiv:2212.04159.

SHU, C.-W. & OSHER, S. 1989 Efficient implementation of essentially non-oscillatory shock-capturing schemes, II. *J. Comput. Phys*. **83** (1), 32–78.

SIMONTE, M., ANDERNACH, H., BRÜGGEN, M., BEST, P.N. & OSINGA, E. 2023 Revisiting the alignment of radio galaxies in the ELAIS-N1 field. *Astron. Astrophys*. **672**, A178.

SURESH, A. & HUYNH, H.T. 1997 Accurate monotonicity-preserving schemes with Runge Kutta time stepping. *J. Comput. Phys*. **136** (1), 83–99.

SYNGE, J.L. 1957 *The Relativistic Gas*. North-Holland.

TORRES-ALBÀ, N. & BOSCH-RAMON, V. 2019 Gamma rays from red giant wind bubbles entering the jets of elliptical host blazars. *Astron. Astrophys*. **623**, A91.

TREMMEL, M., KARCHER, M., GOVERNATO, F., VOLONTERI, M., QUINN, T.R., PONTZEN, A., ANDERSON, L. & BELLOVARY, J. 2017 The Romulus cosmological simulations: a physical approach to the formation, dynamics and accretion models of SMBHs. *Mon. Not. R. Astron. Soc*. **470** (1), 1121–1139.

VAIDYA, B., MIGNONE, A., BODO, G. & MASSAGLIA, S. 2015 Astrophysical fluid simulations of thermally ideal gases with non-constant adiabatic index: numerical implementation. *Astron. Astrophys*. **580**, A110.

VAN LEER, B. 1974 Towards the ultimate conservation difference scheme. II. Monotonicity and conservation combined in a second-order scheme. *J. Comput. Phys*. **14** (4), 361–370.

VAN LEER, B. 1977 Towards the ultimate conservative difference scheme. IV. A new approach to numerical convection. *J. Comput. Phys*. **23**, 276.

https://doi.org/10.1017/S0022377823000892 Published online by Cambridge University Press

VAZZA, F., WITTOR, D., DI FEDERICO, L., BRÜGGEN, M., BRIENZA, M., BRUNETTI, G., BRIGHENTI, F. & PASINI, T. 2023 Life cycle of cosmic-ray electrons in the intracluster medium. *Astron. Astrophys*. **669**, A50.

VIEYRO, F.L., TORRES-ALBÀ, N. & BOSCH-RAMON, V. 2017 Collective non-thermal emission from an extragalactic jet interacting with stars. *Astron. Astrophys*. **604**, A57.

VLAHAKIS, N. & KÖNIGL, A. 2004 Magnetic driving of relativistic outflows in active galactic nuclei. I. Interpretation of parsec-scale accelerations. *Astrophys. J*. **605** (2), 656ï£¡ï£¡661.

WAGNER, A.Y., BICKNELL, G.V. & UMEMURA, M. 2012 Driving outflows with relativistic jets and the dependence of active galactic nucleus feedback efficiency on interstellar medium inhomogeneity. *Astrophys. J*. **757** (2), 136.

WEINBERGER, R., EHLERT, K., PFROMMER, C., PAKMOR, R. & SPRINGEL, V. 2017 Simulating the interaction of jets with the intracluster medium. *Mon. Not. R. Astron. Soc*. **470** (4), 4530–4546.

WYKES, S., CROSTON, J.H., HARDCASTLE, M.J., EILEK, J.A., BIERMANN, P.L., ACHTERBERG, A., BRAY, J.D., LAZARIAN, A., HAVERKORN, M., PROTHEROE, R.J., *et al.* 2013 Mass entrainment and turbulence-driven acceleration of ultra-high energy cosmic rays in Centaurus A. *Astron. Astrophys*. **558**, A19.

WYKES, S., HARDCASTLE, M.J., KARAKAS, A.I. & VINK, J.S. 2015 Internal entrainment and the origin of jet-related broad-band emission in Centaurus A. *Mon. Not. R. Astron. Soc*. **447** (1), 1001–1013.

YATES-JONES, P.M., SHABALA, S.S. & KRAUSE, M.G.H. 2021 Dynamics of relativistic radio jets in asymmetric environments. *Mon. Not. R. Astron. Soc*. **508** (4), 5239–5250.